

Chemical Science

Accepted Manuscript



This is an *Accepted Manuscript*, which has been through the Royal Society of Chemistry peer review process and has been accepted for publication.

Accepted Manuscripts are published online shortly after acceptance, before technical editing, formatting and proof reading. Using this free service, authors can make their results available to the community, in citable form, before we publish the edited article. We will replace this *Accepted Manuscript* with the edited and formatted *Advance Article* as soon as it is available.

You can find more information about *Accepted Manuscripts* in the [Information for Authors](#).

Please note that technical editing may introduce minor changes to the text and/or graphics, which may alter content. The journal's standard [Terms & Conditions](#) and the [Ethical guidelines](#) still apply. In no event shall the Royal Society of Chemistry be held responsible for any errors or omissions in this *Accepted Manuscript* or any consequences arising from the use of any information it contains.

ARTICLE

Mechanism and Active Site of Photocatalytic Water Splitting on Titania in Aqueous Surroundings

Cite this: DOI: 10.1039/x0xx00000x

Wei-Na Zhao^a, Zhi-Pan Liu^{a*}Received,
Accepted

DOI: 10.1039/x0xx00000x

www.rsc.org/

The photocatalytic water splitting is regarded as an important route for generating renewable energy. Here charged-slab first principles calculations integrated with periodic continuum solvation model is utilized to analyze the initiating steps of water splitting on two most common TiO₂ surfaces, namely, rutile (110) and anatase (101) at the solid-water interface. It is found that the first proton removal of water ($\text{H}_2\text{O} + \text{hole}^+ \rightarrow \text{OH} + \text{H}^+$) is sensitive to the crystalline phase and surface. The rutile(110) surface is more active for water splitting with the calculated barrier of O-H bond breaking being 0.2 eV lower compared to that on anatase(101). The higher activity of rutile is not due to the redox level of hole (the position of valence band maximum), but caused by more favorable local bonding geometry of the surface. Unexpectedly, the photogenerated hole does not promote the O-H bond breaking, and the charge transfer occurs after the H₂O dissociation when the surface O nearby the dissociated OH anion trapping the hole. The solvation plays important catalytic role to stabilize and remove protons from the reaction site, which inhibits effectively the charge-recombination of the dissociated OH anion with the proton. The theory presented here shows that the chemical properties of surface play significant role in photocatalytic process and a strategy based on simple structural parameters is proposed towards the design of new photocatalyst.

1. Introduction

Recent years have seen enormous research interests on the direct water splitting using solar light radiation.¹ Among various photoactive materials, titania-based composite is one of the most promising catalysts for water splitting, not least because of the high stability under (violet) radiation and the ability for water oxidation even on TiO₂ alone. To date, one major concern for water splitting on titania polymorphs, the practically utilized photocatalysts, is to identify the active site.² Due to the lack of fundamental understandings on the elementary steps of water splitting, how to design better photocatalyst for direct water splitting remains largely elusive. Theory to clarify the roles of the photo-generated hole, the catalyst surface and solvation as related to the water oxidation kinetics are thus urgently required.

Since the discovery of photocatalytic water splitting on TiO₂,³ much effort has been immediately devoted to search for the active site of TiO₂. The water oxidation reaction can be written as $\text{H}_2\text{O} + \text{hole}^+ \rightarrow 1/2\text{O}_2 + 2\text{H}^+$, which is an extremely difficult reaction under heat-driven conditions and occurs only above +1.23 V vs. SHE under electrochemical conditions. Matsumura et al.⁴ showed that water can be photocatalytically oxidized into oxygen on rutile powder with a fairly high efficiency of 9% (iron(III) ions as the electron acceptor) and the quantum efficiency of oxygen evolution is evaluated to be 17% on rutile particles.⁵ They attribute the high activity to the preferential adsorption of Fe^{III} ions on rutile. Although the rutile phase is believed to possess a higher photoactivity for oxidation,⁶ recent studies from well-controlled nanoscience challenge this view, showing the presence of anatase would enhance

the activity or even dominate the oxidation reaction. For example, Ohno et al.⁷ found a clear synergistic effect of P-25 TiO₂ powder (the proportion of the crystalline phases anatase and rutile is about 4 : 1⁸) for the photocatalytic oxidation of naphthalene. Similarly, Zhang et al.⁹ found that the presence of the phase junction between anatase and rutile can greatly enhance the photocatalytic activity of TiO₂ by up to four times as evidenced by Raman spectroscopy and high-resolution TEM. On the other hand, Kavan et al.¹⁰ synthesized single crystals of TiO₂ anatase containing 0.22% of Al and traces of V, Zr, Nb, and La and found that photoelectrochemical oxidation of water could occur efficiently on both rutile and anatase (with the incident photon at ~ 300 nm), but the reduction of water to H₂ (by photogenerated electrons) proceeded only spontaneously on anatase. Higher photo-oxidation ability of anatase(101) compared to rutile surfaces has also been reported from methanol photo-oxidation on well-defined single-crystal surfaces.¹¹

Theoretical studies would be highly desirable to resolve the kinetics data of water oxidation on various catalyst surfaces. However, such investigations on the solid-liquid interface photocatalysis is rather limited,¹² despite the fact that first principles calculations have been overwhelmingly utilized for predicting the thermodynamic¹³ and kinetics properties¹⁴ of heterogeneous catalysis in the last twenty years. Obviously, this is due to intrinsic complexity arising from the electrical double-layer at the solid-liquid interface and the photo irradiation conditions. There are two critical issues that are important to photocatalysis but not well treated in the conventional density functional theory (DFT) packages, namely, (i) the modelling of the solid-liquid interface that is essential for modelling the strong polarization of the charged surfaces in solution; (ii) the inaccuracy of current DFT functionals in describing the redox

levels of oxides (e.g. the band gap, the valence band position relative to the H₂O/H₂ and H₂O/O₂ levels).¹⁵ These led to a great challenge to compute the photocatalytic reaction kinetics as driven by the excess holes/electrons accumulated on the catalyst surfaces.

Here we report a first theoretical analysis on the mechanism and the possible active site for water oxidation on titania. Large-scale calculations based on the DFT integrated with a periodic continuum solvation model (DFT/CM-MPB method) are utilized for modeling the charge-driven photo-oxidation process at the solid-liquid interface involving two common surfaces of two typical TiO₂ phases, i.e. anatase (101) and rutile (110). We demonstrate that the charged-slab DFT/CM-MPB method allows us to evaluate in detail the water oxidation kinetics and compare the activity across surfaces within a unified theoretical framework, in which the electrical double-layer effect due to the surface charging and the redox level of oxide surfaces can be properly treated simultaneously.

2. Methodology and Calculation Detail

2.1. DFT/CM-MPB methods and surface models

All DFT calculations were performed using SIESTA¹⁶ where optimized double- ζ plus polarization numerical atomic orbital basis sets¹⁷ were utilized along with the Troullier-Martins norm-conserving pseudopotentials.¹⁸ The exchange correlation functional utilized is at the generalized gradient approximation level proposed by Perdew, Burke and Ernzerhof (GGA-PBE).¹⁹ The semi-core 3s and 3p states of Ti were included in all calculations. The cutoff for the real space grid was set as 250 Ry. The L-BFGS method was employed for geometry relaxation until the maximal forces on each relaxed atom were less than 0.1 eV/Å. Finite difference method is utilized to compute the eigenvalues of Hessian and correct the zero point energy (ZPE) of the system. All transition states (TSS) of reaction were searched using Constrained-Broyden-Minimization and Constrained-Broyden-Dimer methods designed for treating complex reaction systems.²⁰

The solid-liquid interface is modeled using a recently-developed periodic CM-MPB method,²¹ which can account for the long-range electrostatic interaction due to solvation between surface and solution. Using the approach, the surface can be charged to mimic the charged surface under photocatalytic conditions and the counter charge is distributed as point charges outside the surface (the vacuum region) in the manner determined by the MPB equation. Such a distribution mimics the realistic electrolyte distribution and is thus more physically meaningful compared to the homogeneous background charge in standard periodic DFT calculation.²² We have recently utilized this approach for modeling electrochemical reaction on metal surfaces²³ and a detailed description on the methodology can be found in our recent work.²⁴ The dielectric constant of bulk water solution is set as 78.36 according to experimental value. Within the CM-MPB framework, it is convenient to align the band position of extended surfaces with the same solution level (e.g., ~15 Å away from the surface).

The rutile (110) and anatase (101) surface are both modeled by a rectangular unit cell of six TiO₂ layer slab with the lattice parameters of (14.834 × 13.145 Å, 360 atoms) and (10.398 × 15.264 Å, 288 atoms), respectively, and the vacuum spacing is generally larger than 30 Å. The DFT optimized lattice parameters are (a=b=3.81, c=9.67 Å) for anatase and (a=b=4.65, c=2.97 Å) for rutile crystal, which agrees well with the experimental lattice (anatase: a=b=3.78, c=9.49 Å; rutile: a=b=4.59, c=2.96 Å). In all calculations, the central two TiO₂ layers are fixed at bulk-truncated positions while the other

layers are allowed to relax. Due to the large unit cell, only Γ -point was utilized. The convergence of the k-point mesh and basis set in calculating the barrier has been checked for key reactions in our recent work.²⁵

It might be mentioned that the hydroxyl groups are present under experimental conditions (aqueous solution).¹⁸ However, the modelling of the likely composition of adsorbed hydroxyl together with water molecules requires the detailed knowledge on the free energy equilibrium of the species on the surface in contact with the aqueous environment, which is highly challenging for theoretical simulation. On the other hand, since the chemical reactions are local, here we utilize the explicit solvation by adding a few water molecules nearby the reactants together with the implicit CM-MPB model that takes into account the long-range solvent polarization to simulate the reactions at the solid-liquid interface. The same hybrid approach has been utilized in the group for understanding a range of electro and photocatalytic reactions on surface²⁴⁻²⁶. We believe that the hybrid approach is able to provide insights into the photocatalytic water oxidation kinetics.

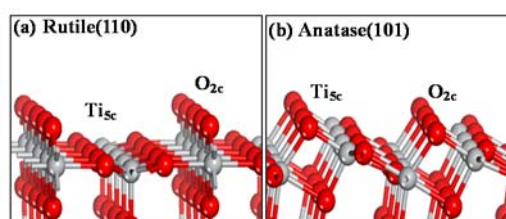


Figure 1. (a) The rutile (110) and (b) the anatase (101) surfaces. Ti, gray; O, red.

2.2 Charged-slab DFT/CM-MPB calculations for band level correction

For photoreaction on semiconducting catalysts, the conduction-band minimum (CBM) and valence-band maximum (VBM) levels of the system are critical, which measure the chemical potential of photo-generated hole/electron and thus determine the thermodynamic tendency for a reaction to occur. Hence, the accurate computation of CBM and VBM levels are the prerequisite for understanding the kinetics of photocatalytic reactions. However, due to the self-interaction problem²⁷ in density functionals, there is a tendency for the delocalization of electrons using local density approximation (LDA) and its generalized gradient extension (GGA), which results in the underestimation of the band gap and the wrong VBM and CBM levels.

Among the attempts devoted to tackle the gap problem of DFT, the recently-developed Δ -sol method²² is an attractive approach, which utilizes the total energy of charged system to deduce the gap ($E_{\text{gap}}=E_{\text{CBM}}-E_{\text{VBM}}$), as written in equation 1-3, without recourse to heavy-demanding high-level quantum mechanics calculations. Analogous to Δ -SCF method for the finite systems that shows improvement for the HOMO-LUMO gap prediction,²⁷⁻²⁸ the Δ -sol method can reasonably avoid the delocalization error by confining the added charge to a volume that is commensurate with the range of the screening effects. The Δ -sol method involves fitted parameters on the system size that were optimized for a set of bulk materials and it cannot be straightforwardly applied to the surface system.

$$E_{\text{gap}}=[E(N_0+n)+E(N_0-n)-2E(N_0)]/n \quad (1)$$

$$E_{\text{VBM}} = [E(N_0 - n) - E(N_0)]/n \quad (2)$$

$$E_{\text{CBM}} = [E(N_0 + n) - E(N_0)]/n \quad (3)$$

We have extended the idea to surface systems where the photocatalytic reactions occur.²⁹ Here we briefly introduce the approach and utilize this method for rutile and anatase surfaces. To extend the Δ -sol method to surface systems, two key issues inherent to the charged-cell calculations must be properly addressed: (1) the image-charge interaction error due to the neutralizing counter-charge required in periodic system calculations; (2) the optimum surface cell size for the added charge on surface. In fact, the first problem can be largely avoided by using DFT-CM/MPB approach, because the neutralizing counter charge is distributed outside the surface region following MPB equation and the large dielectric constant of water can effectively screen the image-charge interaction. To search for the optimum unit cell size for surface system, we can calculate the band structure of a bare oxide surface at different surface charge conditions. Figure 2 shows that with the increase of surface charge, the band gap of rutile and anatase surfaces increases, which is similar to those in finite systems.²²

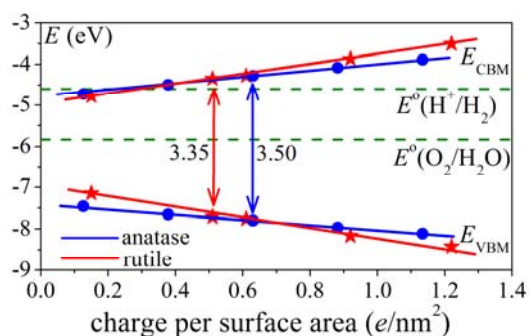


Fig. 2. The variation of the gap (E_{gap}), the level of VBM (E_{VBM}) and the level of CBM (E_{CBM}) with the added charge per surface area for anatase and rutile as calculated from the charged-slab DFT/CM-MPB method. The standard equilibrium potential of H^+/H_2 and $\text{O}_2/\text{H}_2\text{O}$ are also shown for the guide of eye (the absolute potential of SHE is taken at 4.6 V³⁰).

As shown in Figure 2, for both rutile and anatase, a window of the surface charge, i.e. 0.45–0.65 e/nm^2 , can reproduce reasonably the experimental values (rutile: $E_{\text{gap}} \sim 3.0$ eV, $E_{\text{VBM}} \sim 3.0$ V vs. SHE and $E_{\text{CBM}} \sim 0$ V vs. SHE;³¹ anatase: $E_{\text{gap}} \sim 3.2$ eV, $E_{\text{VBM}} \sim 3.0$ V vs. SHE and $E_{\text{CBM}} \sim -0.2$ V vs. SHE^{1d}). For photocatalytic reaction, the local surface charge has to be one (either +1 or -1 of the hole/electron). In view of the 0.45–0.65 e/nm^2 window, it is indicated that only certain size of the unit cell is allowed in order to reproduce the experimental values. In this work, the large rectangle unit cells are selected for anatase (10.398×15.264 Å) with the surface charge density of 0.63 e/nm^2 and rutile (14.834×13.145 Å) with the surface charge density of 0.51 e/nm^2 . These slabs can be explicitly charged by +2 or -2 (two symmetrical surfaces per slab²⁴) and the predicted E_{gap} , E_{VBM} and E_{CBM} for anatase are 3.50 eV, 3.20 V vs. SHE and -0.30 V vs. SHE, and those for rutile are 3.35 eV, 3.11 V vs. SHE and -0.25 V vs. SHE, respectively. These values are generally close to the experimental data. The charged-slab approach allows the quantitative evaluation of the charge-driven reaction kinetics with reasonable VBM and CBM levels.

To further verify the results from the charged DFT/CM-MPB calculations for reaction kinetics, we also utilized the hybrid functionals as implemented in CP2K/QUICKSTEP³² package for

computing the barrier of key reactions. In CP2K, the hybrid functionals, such as HSE06, are available for treating large oxide surface systems thanks to the auxiliary density matrix method³³ for computing the Hartree-Fock exchange. The calculated band gap using above setups for rutile and anatase are 3.12 and 3.62 eV from HSE06 functional, respectively, which are consistent with previous work³⁴ and also compatible with those (3.35 and 3.50 eV) from charged-slab DFT/CM-MPB calculation shown above. In this work, we found that the difference between charged-slab PBE and HSE06 functional in the calculated barrier is generally small (e.g. the barriers of the O-H cleavage differ ~ 0.1 eV using the two functionals, see section 3.2).

2.3. Theoretical approach for calculating the kinetics of photocatalytic reactions

To investigate photocatalytic kinetics on solid surfaces, the most practical approach is to focus on the electron/hole driven redox chemistry assuming that the intra-band deexcitation has taken place after the separation of the photo-generated exciton. This is reasonable as the temporal scale for electron relaxation is \sim ps, being much shorter than that for charge recombination.³⁵ With this assumption, the surface redox chemistry can be considered as the surface reaction occurring in the presence of an excess electron or hole at the solid-liquid interface. This reduces the computational task to model appropriately the charged (not “excited-state”) systems. In this work, the DFT/CM-MPB method is used to calculate the charged surface systems.

Specifically, for a photocatalytic reaction, such as HA dissociation into A and H^+ , we can always decompose the reaction into a number of elementary steps and then calculate the free energy change of the elementary step. For example, for the charging of an adsorbed HA molecule on surface (HA/sur) by a photo-generated hole, $\text{HA/sur} + \text{h}^+ \rightarrow [\text{HA/sur}]^+$; The free energy change ΔG can be calculated by

$$\Delta G_I = G([\text{HA/sur}]^+) + G(\text{sur}) - G(\text{sur}^+) - G(\text{HA/sur}) \quad (4)$$

where the term $(G(\text{sur}^+) - G(\text{sur}))$ divided by Faraday constant, i.e. $(G(\text{sur}^+) - G(\text{sur}))/F$ should be the absolute electrostatic potential of hole (U_h) at VBM of the surface, which can be obtained from the charged-slab DFT/CM-MPB calculations, as detailed above. In this work, U_h is determined to be 2.80 V for rutile(110) and 3.20 V for anatase(101) vs. SHE according to $G(\text{sur}) - G(\text{sur}^+)$, where the surface structural relaxation in the presence of hole are also considered. Obviously, a realistic estimation of VBM and thus U_h is a must for evaluate the activity of the photocatalytic oxidation (otherwise the computed reaction barrier will be incorrect due to the wrong chemical potential of hole).

For the reactions involving H^+ , e.g. $[\text{H/sur}]^+ \rightarrow \text{sur} + \text{H}^+(\text{aq})$, the free energy change ΔG can be calculated by

$$\begin{aligned} \Delta G_2 &= G(\text{H}^+_{\text{aq}}) + G(\text{sur}) - G([\text{A+H/sur}]^+) \\ &= 1/2G(\text{H}_2) + 4.6 \text{ eV} + G(\text{sur}) - G([\text{A+H/sur}]^+) \end{aligned} \quad (5)$$

where the free energy change in the SHE reference electrode is utilized

$$\Delta G_{\text{SHE}} = 1/2G(\text{H}_2) - G(\text{H}^+_{\text{aq}}) + 4.6 \text{ eV} = 0 \quad (6)$$

3. Results

For water oxidation, the first proton removal ($\text{H}_2\text{O}^* + \text{hole}^+ \rightarrow \text{OH}^* + \text{H}^+(\text{aq})$; hereafter the subscript * indicates the adsorbed state) is known to be the key kinetic step (see our previous work³⁶ where the overall mechanism of water oxidation is computed from thermodynamics and compared with experimental observations^{2b}), which involves both the O-H bond breaking and the hole transfer. In this work, we will quantify the kinetics of this step on two TiO_2 surfaces and compare the activity difference between the two surfaces. There are three likely routes for the first proton removal, which differs in the sequence of the O-H bond breaking and the charge transfer, as outlined below.

- Hole-promoted water dissociation: the charge (hole) transfers from bulk to adsorbed water that leads its subsequent dissociation, i.e. $\text{H}_2\text{O}^* + \text{hole}^+ \rightarrow \text{H}_2\text{O}^{*+} \rightarrow \text{OH}^* + \text{H}^{*+}$; In this route, the hole promotes the water dissociation.
- Homolytic water splitting: water dissociates homolytically followed by the charge transfer from bulk to the adsorbed H, i.e. $\text{H}_2\text{O}^* \rightarrow \text{OH}^* + \text{H}^*$; $\text{H}^* + \text{hole}^+ \rightarrow \text{H}^{*+}$;
- Heterolytic water splitting: water dissociates heterolytically followed by the charge transfer from bulk to adsorbed OH, i.e. $\text{H}_2\text{O}^* \rightarrow \text{OH}^{*+} + \text{H}^{*+}$; $\text{OH}^{*+} + \text{hole}^+ \rightarrow \text{OH}^*$;

3.1 The adsorbed species and their relative band position

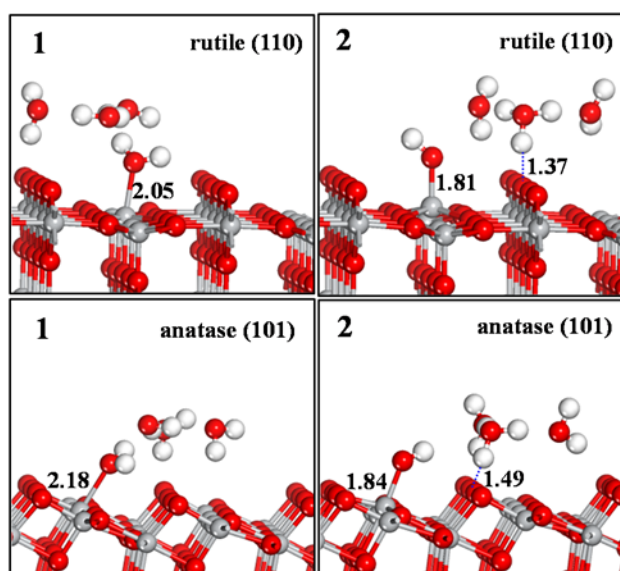


Figure 3. Optimized structures of the adsorbed (state 1) and the dissociated (state 2) H_2O states on rutile (110) and anatase (101) surface in aqueous solution. Three water molecules are included as the explicit first shell solvation and the rest of solution is represented using CM-MPB method. Key structural parameters (Å) are labelled. Ti, gray; O, red; H, white.

To provide insights into the mechanism and the kinetics, we have first calculated the geometrical and electronic structure of the initial state (IS) and the possible final states (FS) of the first proton removal reaction, namely, the adsorbed H_2O , the coadsorbed OH and H (dissociated H_2O) at the solid-liquid interface. Due to the three possible reaction routes as mentioned above, the surfaces considered for these IS and FSs are either neutral or positively-charged (with hole). The optimized structures of the adsorbed H_2O (state 1) and the

dissociated H_2O (state 2) in aqueous solution (with both explicit and implicit H_2O solvation) are shown in Figure 3.

For H_2O adsorption, water adsorbs perpendicularly on a surface five-coordinated Ti (Ti_{5c}) site via its O end forming a O- Ti_{5c} bond, consistent with the previous calculations.^{37,38} The other water molecules nearby the adsorbed H_2O interact with the adsorbed H_2O and the lattice O through the hydrogen bonding, which are ~ 2.50 Å above the surface forming the weakly-bound water layer. Compared to that on the neutral surface, the O- Ti_{5c} distance is shortened slightly on the positively-charged surface, indicating an increased O-Ti bonding due to the electrostatic interaction. Next, we calculated the adsorption free energy of the H_2O on the surface, which is defined by $\Delta G = G(\text{X}/\text{sur}) - G(\text{X}) - G(\text{sur})$, where G is the free energy of the system based on DFT/CM-MPB calculations under the conditions of interest (e.g. vacuum, solution or charged surface). In accordance with the structural change, we found that the adsorption free energy of water without and with the surface hole are -0.86 and -1.01 eV, respectively. The results for H_2O on anatase (101) is quite similar to those on rutile (110), both in structure and in energetics, as summarized in Table 1.

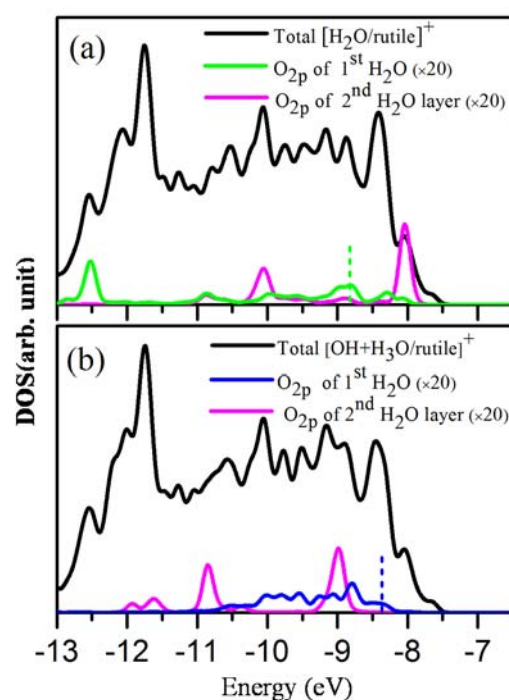


Figure 4. The total (TDOSs, black curve) and the projected density of states (PDOSs) for (a) the adsorbed H_2O ; and (b) the dissociated H_2O on the charged rutile(110) in aqueous solution (via CM-MPB). 1st H_2O : the adsorbed H_2O on surface; 2nd H_2O : the H_2O molecules at the second layer. Green: the O 2p states of the adsorbed H_2O ; Blue: the O 2p states of the OH anion from the dissociated H_2O ; Pink: the O 2p states of the H_2O molecules nearby the dissociating H_2O . The dotted lines indicate the major occupied O 2p states of the adsorbed H_2O or OH that are just below the VBM.

In Figure 4, we showed the calculated total and projected density of states (DOS) of the adsorbed H_2O on rutile(110) surface in the presence of hole. We found that the VBM of rutile(110) (~ -7.5 eV) is mainly contributed from the lattice O atoms on the surface, not from the adsorbed H_2O molecules. The major occupied O_{2p}

states of the adsorbed H₂O molecule (~8.8 eV) is ~1.3 eV lower compared to the VBM level of TiO₂ (also listed in Table 1). This indicates that the hole transfer from the surface (lattice O) to the adsorbed H₂O molecules is highly activated and is thus unlikely. For the weakly-bound water layer, their O atom 2p states (~7.8 eV) are closer but still below the VBM.

For the dissociated H₂O, the coadsorbed OH and H, we found that the OH also prefers to adsorb at the Ti_{5c} and the H will first attach to the two-coordinated bridging O (O_{2c}) on both rutile and anatase surfaces. However, once introducing the explicit water molecules above the H (e.g. with three water molecules above), the formation of a solvated proton (e.g. (H₂O)₂-H₃O) is spontaneous from the energy minimization. The formation of the solvated proton occurs on both rutile and anatase, and is also independent on the surface charge condition. The solvated proton has one of its H interacting with the bridging O_{2c} (see Figure 3). This is consistent with the strong acidity of the TiO₂-H⁺ species (the calculated pKa of TiO₂-H⁺ → TiO₂+H⁺ is -1 for rutile³⁹). Our electronic structure analysis confirms that the (H₂O)₂-H₃O accumulates one positive charge, indicating the formation of the solvated proton and thus the tendency of the immediate charge separation after water dissociation at the oxide/water interface. Since the state of OH*+H⁺ is the only possible FS for the first proton removal reaction, we can therefore rule out the homolytic water splitting channel, route (ii), proposed above.

Table 1. The calculated free energy G of the key states in the first proton removal reaction of H₂O oxidation on rutile and anatase in aqueous solution. All free energies are with reference to the clean surface and the water in aqueous solution.

| State* | G (eV) | $d_{\text{O-Ti}}$ (Å) | ΔE_{band} (eV) [#] |
|----------------------|----------|-----------------------|--|
| Rutile (110) | | | |
| 1 | -0.86 | 2.05 | -1.3 |
| 1 ⁺ | -1.01 | 2.04 | -1.2 |
| 2 | -1.03 | 1.81 | -0.8 |
| 2 ⁺ | -1.36 | 1.79 | -0.8 |
| Anatase (101) | | | |
| 1 | -0.60 | 2.18 | -1.3 |
| 1 ⁺ | -0.75 | 2.15 | -1.3 |
| 2 | -0.73 | 1.84 | -0.5 |
| 2 ⁺ | -0.90 | 1.81 | -0.5 |

*1: adsorbed H₂O; 1⁺: adsorbed H₂O on positively-charged surface; 2: adsorbed OH and H; 2⁺: adsorbed OH and H on positively-charged surface.

[#] ΔE_{band} : the band position of the O_{2p} of the adsorbed H₂O or OH with respect to the TiO₂ VBM (see Figure 4)

In Figure 4b, we also compared the calculated total and projected DOS of dissociated H₂O on rutile(110) surface in the presence of hole, where the OH adsorbs on surface and the H is present as a solvated proton in the water layer. The total DOS of the OH*+H⁺ state is quite similar to that of the H₂O adsorbed state except that the O_{2p} state of the adsorbed OH species is obviously more active than that of the adsorbed water molecule. The O_{2p} position of the adsorbed OH is ~0.8 eV below VBM of rutile, and thus ~0.5 eV above that of the adsorbed water molecule (c.f Figure 4a and b). The O_{2p} states of the H₃O⁺ is much lower in energy, ~1.5 eV below VBM in rutile, indicating that the solvated proton is already very stable and should not accept hole from the surface.

We now summarize the calculated results for adsorbed H₂O and OH+H⁺ states on rutile and anatase in Table 1. We found that rutile generally binds more strongly for the ISs and the FSs. This can be attributed to the stronger Ti-O bond, as indicated by the shorter Ti-O bond distance on rutile. For the electronic structure, the relative band position of the species on rutile and anatase are quite similar. It is noted that the OH species has a more active O_{2p} states (their band position closer to the VBM) compared to the adsorbed H₂O molecule. Nevertheless, neither the adsorbed OH anions nor the adsorbed H₂O is likely to act as a hole trapper. Instead, the lattice Os on the surface nearby the adsorbed H₂O or OH anion could be the potential hole trapper due to the enhanced electrostatic interaction between the trapped hole and the adsorbed H₂O or OH.

From the calculated energetics and band position of the adsorbed O-containing species, we can rule out the homolytic H₂O dissociation mechanism since the solvated proton are the only possible final product from the first proton removal reaction. In the following, the kinetics analysis on the route (i) and (iii) are performed to identify the most favorable pathway.

3.2 Water dissociation with and without the hole

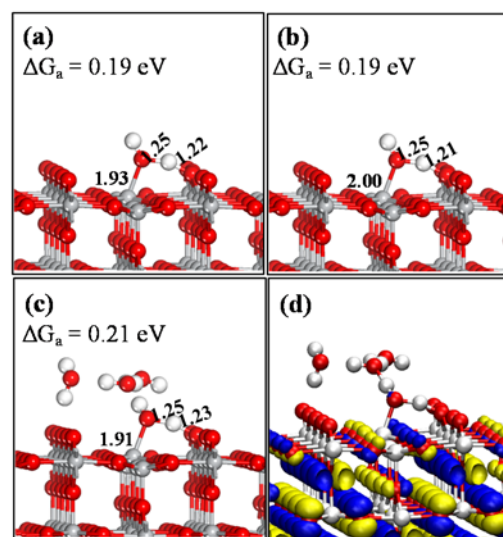


Figure 5. The calculated TS and barrier (ΔG_{a} , eV) for H₂O dissociation on rutile(110) surface under different conditions. (a). on charged surface (with hole) in aqueous solution (CM-MPB); (b) on neutral surface (without hole) in aqueous solution (CM-MPB). (c) on neutral surface (without hole) in aqueous solution (with both implicit and explicit solvation). (d) 3D isosurface contour plots of the HOMO for the TS of H₂O splitting (both the hybrid HSE06 and PBE functional provide the consistent picture). The isosurface value is set as $\pm 0.02 \text{ e}/\text{\AA}^3$. Key structural parameters (Å) are labelled. Ti, gray; O, red; H, white.

Since route (i) and route (iii) differ mainly in the mechanism of H₂O dissociation, i.e. whether the hole directly participates in the O-H bond breaking of the adsorbed H₂O, we have utilized the charged-slab DFT/CM-MPB method to investigate the water dissociation kinetics in the presence and absence of the hole. From the above section, we show that the hole transfer is thermodynamically unfavorable since the VBM of TiO₂ is far above the O_{2p} level of adsorbed H₂O molecule (the IS). It is thus expected that the electronic structure of the TS of the OH-bond breaking should

determine largely whether the presence of hole can assist the H₂O dissociation.

On rutile(110) and anatase(101) surface, we first searched for the TS of the O-H bond breaking of one H₂O molecule in vacuum condition on the charged surface, which serve as the benchmark to compare the energetics using different DFT functionals. We found that using PBE functional the dissociation barrier is 0.22 eV and 0.60 eV (without ZPE correction) on rutile and anatase, respectively. The correction to the barrier are +0.13 eV and +0.08 eV for the reaction on the two surfaces, by switching the functional from PBE to the hybrid functional HSE06. This is reasonable as the pure DFT functional tends to underestimate the reaction barrier.⁴⁰ Since the error introduced by the functional is not large, i.e. ~0.1 eV within the typical systematic error of DFT calculations, it indicates that the O-H bond breaking kinetics concerned here is in fact not sensitive to DFT functional and below we will use PBE functional mainly in combination with the charged-slab DFT/CM-MPB method for investigating the H₂O dissociation on different surfaces.

Next, we examined the influence of the surface hole on the barrier of the H₂O dissociation in aqueous solution via the CM-MPB model. On the neutral surface, the H₂O dissociation free energy barrier is calculated to be 0.19 eV on rutile and 0.39 eV on anatase in aqueous solution. The barrier remains essentially the same when the surface is positively charged (with hole), i.e. 0.19 eV and 0.38 eV on the two surfaces. These calculated TSs on rutile are shown in Figure 5a and b. Obviously, the presence of the surface hole does not influence much on the barrier of O-H breaking. Instead, the surface structure is critical to the O-H bond breaking. Using Microkinetics and assuming the same preexponential factor, it can be estimated that the water splitting on rutile is 3 orders of magnitude faster than it on anatase at the ambient conditions (300 K).

To further examine the possible contribution of the short-range polarization due to the explicit solvation, we also added three explicit H₂O molecules nearby the dissociating H₂O molecule and re-searched the IS and the TS for the H₂O dissociation reaction on the neutral surfaces. The calculated TS is shown in Figure 5c and the barrier is found to be 0.21 eV on rutile, which are also similar to their counterparts without the explicit H₂O solvation. This indicates that the CM-MPB model can describe well the kinetics of the O-H bond breaking of adsorbed H₂O, where the oxide surface with positive Ti and negative O atoms interact strongly with the dissociating TS complex.

It is important to ask why the presence of surface hole does not promote the O-H bond breaking of H₂O molecule. To this end, we have analyzed the electronic structure of the O-H bond breaking TS. Shown in Figure 5d is the 3D isosurface contour plots of the VMB (HOMO) for the TS (PBE and HSE06 functional provides the consistent picture). On both rutile (110) and anatase (101), we found that the spatial distributions of the hole locate mainly on the surface (lattice O), not on the TS complex. This explains qualitatively why the presence of hole does not promote the O-H bond breaking.

Quantitatively, we can also interpret the influence of the hole on the reaction barrier of O-H bond breaking according to the partial derivative, $\partial E_a/\partial n$, where n is the number of electron in the system. The $\partial E_a/\partial n$ can be expressed as a function of the eigenvalue of HOMO (ϵ_{HOMO}) at the IS and the TS, as derived in eq. 7 and 8.

$$\frac{\partial E_a}{\partial n} = \frac{E_a(N) - E_a(N-\Delta n)}{\Delta n} = \frac{E_{\text{TS}}(N) - E_{\text{TS}}(N-\Delta n)}{\Delta n} - \frac{E_{\text{IS}}(N) - E_{\text{IS}}(N-\Delta n)}{\Delta n} \quad (7)$$

$$\frac{\partial E_a}{\partial n} \approx \epsilon_{\text{HOMO}}(\text{TS}) - \epsilon_{\text{HOMO}}(\text{IS}) = \Delta \epsilon_{\text{HOMO}} \quad (8)$$

where Δn is the change of the number of electron in the system, and $\frac{E(N) - E(N-\Delta n)}{\Delta n} \approx \epsilon_{\text{HOMO}}$ based on DFT theorem, which states that HOMO is the derivative of the free energy of electron (G) to the number of electrons (N).⁴¹ Eq. 8 shows that the smaller change for the HOMO level from the IS to the TS ($\Delta \epsilon_{\text{HOMO}}$) at the charge-neutral condition (i.e. $n=0$) is, the smoother the slope of the barrier against the number of electron would be. From our calculations, we found that the $\Delta \epsilon_{\text{HOMO}}$ for rutile and anatase are rather small, only -0.05 and 0.03 eV, respectively. This indicates that the barrier is not sensitive to the change of the number of electron in the system, as indeed found from the calculated barriers with and without the hole.

3.3 The overall mechanism

The above results show that the H₂O dissociation is activated on TiO₂ surfaces and cannot be promoted by the surface hole. It is therefore reasonable that the capture of hole occurs after the dissociation of H₂O. It is the final state of the H₂O dissociation, i.e. the OH anion and the solvated proton, state **2**, that captures a hole to form the state **2**⁺. In the state **2**⁺, the hole may be transferred to OH anion to form OH radical or be trapped on the lattice O nearby the OH anion. According to the electronic structure shown in Figure 4b, the latter picture could be thermodynamically more likely.

The overall mechanism of the first proton removal of water on TiO₂ can thus be described by two elementary steps, (1) heterolytic H₂O dissociation, H₂O/sur → [H---OH]/sur → OH⁻/sur + H₃O⁺(aq); and (2) the hole transfers to the surface O nearby the adsorbed OH anion; OH⁻*/sur + hole⁺ → [OH/sur]. Based on the charged-slab DFT/CM-MPB calculations, we have obtained the reaction free energy profile on rutile (110) and anatase(101), as shown in Figure 6.

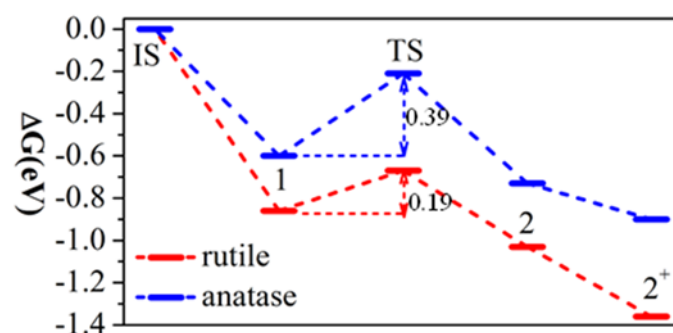


Figure 6 Free energy profiles for the first proton removal reaction in photocatalytic H₂O splitting on rutile (110) and anatase (101) surfaces.

Figure 6 shows that the first proton removal reaction occurs more favorably on the rutile surface compared to that on the anatase surface. The overall energetics can be summarized as follows. The adsorption of H₂O on rutile (110) (state **1**) is exothermic by 0.86 eV, which is 0.26 eV lower than that on anatase(101) with respect to H₂O in solution. The free energy barrier of H₂O dissociation is 0.19 eV on rutile and 0.39 eV on anatase. The charge transfer occurs after the H₂O dissociation, i.e. **2** + hole⁺ → **2**⁺, with the free energy change being -0.33 eV and -0.17 eV on rutile and anatase, respectively. Compared to it on anatase, the final state **2**⁺ on rutile is better stabilized. Overall, this photocatalytic deprotonation reaction, i.e. H₂O* + hole⁺ → OH* + H⁺(aq), is exothermic by 0.50 eV on rutile (110) and 0.30 eV on

anatase (101). It is clear that the photocatalytic water splitting occurs preferentially on rutile, not on anatase.

4. Discussion

Our results show that the key elementary step of the first proton removal for water oxidation is the O-H bond breaking, which is an activated process even at the high overpotential condition of TiO₂ (i.e. with the ultraviolet radiation). Importantly, the reaction is surface structure sensitive and the activity of rutile is much higher. The calculated results support the conventional view that the rutile phase is more active than anatase for water oxidation.

From the electronic structure, we can rule out that the position of VBM is the cause for the enhanced photoactivity of rutile surface compared to that of anatase surface. By adding/subtracting the hole in the reaction, we found that the presence of the hole that is present at the VBM of the oxide surfaces at the ISs in fact does not promote the O-H bond breaking. The hole does not have a significant spatial distribution on the O-H bond breaking TS complex. This finding is important, implying that the current DFT functionals could provide good energetics for the water oxidation reaction, as also confirmed from the barriers using the PBE functional and the HSE06 functional.

It is natural to ask then what cause the surface structure sensitivity for the O-H bond breaking. We first evaluated the stability for the adsorbed H on the bridging O_{2c} on rutile(110) and on anatase (101), considering that the bridging O accept the H during the O-H bond breaking. By using the charged-slab DFT/CM-MPB calculations, we found that the adsorption free energy of H⁺ on the both surfaces are almost identical, i.e., ~0.15 eV. This indicates that the Lewis basicity of the oxide lattice O_{2c} are similar and should not be the cause for the activity difference between the surfaces.

Next, we compared the adsorption of H₂O and OH on rutile(110) and anatase(101) surface. From Table 1, we can see that the H₂O states and the dissociated OH/H⁺ states are generally more stable on rutile compared to them on anatase. Overall, the dissociation of H₂O on rutile (i.e. **1**→**2**) is only slightly more favorable (0.17 eV on rutile vs. 0.13 eV on anatase). Considering much larger barrier difference (~0.2 eV) for the O-H bonding breaking between on rutile and on anatase, the thermodynamics only cannot fully explain to the activity difference.

Table 2. The distance (Å) between the Ti_{5c} cation and its nearest O_{2c} anion of the TiO₂ surfaces. The data is taken from the surfaces that can expose only the Ti_{5c} cations and O_{2c} anions.

| | Rutile | Anatase | Brookite | TiO ₂ (II) |
|-------|--------|---------|----------|-----------------------|
| (110) | 3.53 | / | 3.45 | 3.21 |
| (101) | 3.52 | 3.92 | | / |
| (111) | 4.13 | / | 3.45 | 3.21 |
| (100) | 4.13 | 4.34 | 3.67 | 3.50 |
| (010) | 4.13 | 4.33 | / | / |
| (011) | 3.52 | 3.92 | / | / |
| (001) | / | 4.31 | 3.72 | 3.64 |
| (112) | / | 4.32 | / | / |

By closely inspecting the calculated TS of H₂O dissociation, we can finally attribute the higher activity of rutile to the more favorable local geometrical structure, which can better stabilize the TS of the

O-H bond breaking. On rutile(110), we found that the distance between the exposed Ti_{5c} and the O_{2c} is 3.53 Å, whilst it is 3.92 Å on anatase(101) (also see Figure 1). As a result, the distance between the O (in H₂O) and the lattice O_{2c} on rutile(110) is 2.46 Å at the TS, which is 0.05 Å shorter than that on anatase(101). Consistently, the distance between the O (in H₂O) and the Ti_{5c} is 1.93 Å at the TS (Figure 5a), which is 0.16 Å shorter than that on anatase(101). Therefore, the water molecule can dissociate with a more favorable geometry on rutile, in which the TS complex has a better contact with both the Ti_{5c} (bonding with OH) and the O_{2c} (bonding with H). We suggest that the surface structure sensitivity of water oxidation can be correlated to the geometrical separation between the exposed Ti_{5c} cation and its nearest O_{2c} anion, d_{Ti_{5c}-O_{2c}}, on the surface.

The d_{Ti_{5c}-O_{2c}} as a simple geometrical descriptor may be utilized to rationalize the experimental debate on the active of water oxidation on TiO₂. Using the bulk-truncated structure, we have measured d_{Ti_{5c}-O_{2c}} for a series of common low-miller TiO₂ surfaces, including those from rutile,⁴² anatase,⁴³ brookite⁴⁴ and TiO₂(II) phases,⁴⁵ as shown in Table 2. Interestingly, we found that in addition to rutile(110), the rutile (101) (equivalent (011)) and (001) surfaces also exhibit the short d_{Ti_{5c}-O_{2c}}, indicating that these surfaces could be good candidates as the active site for water splitting. Indeed, Ohno et al.,⁴⁶ with the scanning electron microscopy, have observed that rutile (011) shows high activity for water oxidation (PtCl₆²⁻ as the electron acceptor).

It should be pointed out that the other phases of TiO₂ may possess even higher photoactivity for water splitting based on the structural parameter, d_{Ti_{5c}-O_{2c}}. From Table 2, we found that the TiO₂(II) phase has the shortest d_{Ti_{5c}-O_{2c}} on its (110), (111) surfaces among the surfaces/phases investigated. In particular, the (111) surface is known to be the most stable surface of TiO₂(II) according to the experiment and also our own calculations. This finding may help to understand the experimental findings on the enhanced photoactivity on TiO₂ composite containing multiple phases. For example, Zhang et al.⁹ have found that the photocatalytic activity of TiO₂ can be enhanced up to four times with respect to the pure phase. The composite catalyst could contain a variety of active sites with different local geometry, which could provide more favorable local bonding environment for H₂O adsorption and splitting. Further studies along this line are needed to resolve the active site from the atomic level in TiO₂ composite catalysts.

Conclusions

This work represents a first theoretical attempt to resolve the kinetics of the key step of photocatalytic water oxidation, H₂O+hole⁺→OH+H⁺, on two important TiO₂ surfaces of rutile and anatase. To correctly compute the kinetics of the H₂O dissociation under the photocatalytic condition in the aqueous solution, the charged-slab DFT/CM-MPB is developed and utilized to correct the band levels of oxide and simultaneously take into account the electrical double-layer effect at the solid-liquid interface. The theoretical results have been thoroughly compared with experiment and high-level hybrid functional HSE06 calculations. Theory shows that the photocatalytic water splitting on TiO₂ is both surface- and phase-sensitive, and the design of new catalyst towards efficient photocatalytic water splitting can be facilitated by focusing on the catalytic ability of the surface for water O-H bond breaking. Our main results are outlined as follows.

- (i) The rutile(110) surface is more active for water splitting kinetically compared to anatase(101), with the calculated barrier of O-H bond breaking on rutile being ~0.2 eV lower

than it on anatase. The higher activity of rutile is not due to the redox level of hole (the position of valence band maximum), but caused by the more favorable local bonding geometry of the surface, which reduces the barrier of the O-H bond breaking.

- (ii) The photogenerated hole cannot promote the O-H bond breaking and the O-H bond splitting of water is basically a surface-catalytic reaction driven by heat only. The hole transfer occurs after the H₂O dissociation when the surface O nearby the dissociated OH anion trapping the hole.
- (iii) The solid/liquid interface plays important catalytic role to stabilize and remove protons from the reaction site, which avoids effectively the charge-recombination of the dissociated OH anion with the nascent proton.

Acknowledgements

We acknowledge the National Science Foundation of China (21173051, 21361130019), 973 program (2011CB808500, 2013CB834603), Science and Technology Commission of Shanghai Municipality (08DZ2270500), and Program for Professor of Special Appointment (Eastern Scholar) at Shanghai Institute of Higher Learning for financial support.

Notes and references

^a Shanghai Key Laboratory of Molecular Catalysis and Innovative Materials, Department of Chemistry, Key Laboratory of Computational Physical Science (Ministry of Education), Fudan University, Shanghai 200433

* email: zpliu@fudan.edu.cn

- (a)M. A. Henderson, *Surf. Sci. Rep.*, 2011, **66**, 185; (b)J. Tang, J. R. Durrant and D. R. Klug, *J. Am. Chem. Soc.*, 2008, **130**, 13885; (c)C. Gomes Silva, R. Juárez, T. Marino, R. Molinari and H. García, *J. Am. Chem. Soc.*, 2010, **133**, 595; (d)M. Gratzel, *Nature*, 2001, **414**, 338; (e)Z. Yi, J. Ye, N. Kikugawa, T. Kako, S. Ouyang, H. Stuart-Williams, H. Yang, J. Cao, W. Luo, Z. Li, Y. Liu and R. L. Withers, *Nat. Mater.*, 2010, **9**, 559; (f)K. Maeda and K. Domen, *J. Phys. Chem. Lett.*, 2010, **1**, 2655; (g)K. I. Hadjiivanov and D. G. Klissurski, *Chem. Soc. Rev.*, 1996, **25**, 61.
- (a)G. Giorgi, M. Palumbo, L. Chiodo and K. Yamashita, *Phys. Rev. B*, 2011, **84**, 073404; (b)R. Nakamura and Y. Nakato, *J. Am. Chem. Soc.*, 2004, **126**, 1290; (c)A. Imanishi, T. Okamura, N. Ohashi, R. Nakamura and Y. Nakato, *J. Am. Chem. Soc.*, 2007, **129**, 11569.
- A. Fujishima and K. Honda, *Nature*, 1972, **238**, 37.
- T. Ohno, D. Haga, K. Fujihara, K. Kaizaki and M. Matsumura, *J. Phys. Chem. B*, 1997, **101**, 6415.
- K. Fujihara, T. Ohno and M. Matsumura, *J. Chem. Soc., Faraday Trans.*, 1998, **94**, 3705.
- (a)T. Ohno, K. Fujihara, K. Sarukawa, F. Tanigawa and M. Z. Matsumura, *Phys. Chem.*, 1999, **213**, 165; (b)S. J. Tan, H. Feng, Y. F. Ji, Y. Wang, J. Zhao, A. D. Zhao, B. Wang, Y. Luo, J. L. Yang and J. G. Hou, *J. Am. Chem. Soc.*, 2012, **134**, 9978.
- T. Ohno, K. Sarukawa, K. Tokieda and M. Matsumura, *J. Catal.*, 2001, **203**, 82.
- R. I. Bickley, T. Gonzalez-Carreño, J. S. Lees, L. Palmisano and R. J. D. Tilley, *J. Solid State Chem.*, 1991, **92**, 178.
- J. Zhang, Q. Xu, Z. Feng, M. Li and C. Li, *Angew. Chem. Int. Edit.*, 2008, **47**, 1766.
- L. Kavan, M. Grätzel, S. E. Gilbert, C. Klemenz and H. J. Scheel, *J. Am. Chem. Soc.*, 1996, **118**, 6716.
- A. Y. Ahmed, T. A. Kandiel, T. Oekermann and D. Bahnemann, *J. Phys. Chem. Lett.*, 2011, **2**, 2461.
- S. Y. Chen and L. W. Wang, *Chem. Mat.*, 2012, **24**, 3659.
- (a)A. Valdés, Z. W. Qu, G. J. Kroes, J. Rossmeisl and J. K. Nørskov, *J. Phys. Chem. C*, 2008, **112**, 9872; (b)A. Valdés and G. J. Kroes, *J. Phys. Chem. C*, 2010, **114**, 1701; (c)U. Aschauer, Y. He, H. Cheng, S.-C. Li, U. Diebold and A. Selloni, *J. Phys. Chem. C*, 2009, **114**, 1278.
- (a)Q. Guo, C. Xu, Z. Ren, W. Yang, Z. Ma, D. Dai, H. Fan, T. K. Minton and X. Yang, *J. Am. Chem. Soc.*, 2012, **134**, 13366; (b)A. Tilocca and A. Selloni, *J. Chem. Phys.*, 2003, **119**, 7445; (c)C. Sun, L.-M. Liu, A. Selloni, G. Q. Lu and S. C. Smith, *J. Mater. Chem.*, 2010, **20**, 10319.
- (a)A. Fujishima, X. Zhang and D. A. Tryk, *Surf. Sci. Rep.*, 2008, **63**, 515; (b)R. Beranek, *Adv. Phys. Chem.*, 2011, 1.
- J. M. Soler, E. Artacho, J. D. Gale, A. Garcia, J. Junquera, P. Ordejón and D. Sanchez-Portal, *J. Phys: Condens. Matter*, 2002, **14**, 2745.
- J. Junquera, Paz, D. Sánchez-Portal and E. Artacho, *Phys. Rev. B*, 2001, **64**, 235111.
- N. Troullier and J. L. Martins, *Phys. Rev. B*, 1991, **43**, 1993.
- J. P. Perdew, K. Burke and M. Ernzerhof, *Phys. Rev. Lett.*, 1996, **77**, 3865.
- (a)H.-F. Wang and Z.-P. Liu, *J. Am. Chem. Soc.*, 2008, **130**, 10996; (b)C. Shang and Z.-P. Liu, *J. Chem. Theory Comput.*, 2010, **6**, 1136; (c)X.-J. Zhang, C. Shang and Z.-P. Liu, *J. Chem. Theory Comput.*, 2013, **9**, 5745.
- (a)J. L. Fattbert and F. Gygi, *Phys. Rev. B*, 2006, **73**, 115124; (b)J.-L. Fattbert and F. Gygi, *Int. J. Quantum Chem.*, 2003, **93**, 139; (c)H.-F. Wang and Z.-P. Liu, *J. Phys. Chem. C*, 2009, **113**, 17502.
- M. K. Y. Chan and G. Ceder, *Phys. Rev. Lett.*, 2010, **105**, 196403.
- Y.-H. Fang and Z.-P. Liu, *J. Am. Chem. Soc.*, 2010, **132**, 18214.
- Y.-H. Fang, G.-F. Wei and Z.-P. Liu, *Catal. Today*, 2013, **202**, 98.
- Y.-F. Li and Z.-P. Liu, *Phys. Chem. Chem. Phys.*, 2013, **15**, 1082.
- (a)Y.-H. Fang, G.-F. Wei and Z.-P. Liu, *J. Phys. Chem. C*, 2013, **117**, 7669; (b)D. Chen, Y. H. Fang and Z. P. Liu, *Phys. Chem. Chem. Phys.*, 2012, **14**, 16612.
- P. Mori-Sánchez, A. J. Cohen and W. Yang, *Phys. Rev. Lett.*, 2008, **100**, 146401.
- A. J. Cohen, P. Mori-Sánchez and W. Yang, *Phys. Rev. B*, 2008, **77**, 115123.
- Y. F. Li and Z. P. Liu, *Phys. Chem. Chem. Phys.*, 2013, **15**, 1082.
- S. Trasatti, *Electrochim. Acta*, 1991, **36**, 1659.
- J. Cheng and M. Sprik, *Phys. Rev. B*, 2010, **82**, 081406.
- J. Vandevondele, M. Krack, F. Mohamed, M. Parrinello, T. Chassaing and J. Hutter, *Comput. Phys. Commun.*, 2005, **167**, 103.
- M. Guidon, J. R. Hutter and J. Vandevondele, *J. Chem. Theory Comput.*, 2010, **6**, 2348.
- (a)M. E. Arroyo-De Dompablo, A. Morales-García and M. Taravillo, *J. Chem. Phys.*, 2011, **135**, 054503; (b)F. Labat, P. Baranek, C. Domain, C. Minot and C. Adamo, *J. Chem. Phys.*, 2007, **126**, 154703.
- Y. Tamaki, A. Furube, M. Murai, K. Hara, R. Katoh and M. Tachiya, *J. Am. Chem. Soc.*, 2005, **128**, 416.
- Y. F. Li, Z. P. Liu, L. L. Liu and W. G. Gao, *J. Am. Chem. Soc.*, 2010, **132**, 13008.
- F. Allegretti, S. O'Brien, M. Polcik, D. I. Sayago and D. P. Woodruff, *Phys. Rev. Lett.*, 2005, **95**, 226104.
- P. M. Kowalski, B. Meyer and D. Marx, *Phys. Rev. B*, 2009, **79**, 115410.
- J. Cheng and M. Sprik, *J. Chem. Theory Comput.*, 2010, **6**, 880.
- (a)J. P. Perdew and A. Zunger, *Phys. Rev. B*, 1981, **23**, 5048; (b)Y. Zhang and W. Yang, *J. Chem. Phys.*, 1998, **109**, 2604; (c)J.-W. Song, T. Hirotsawa, T. Tsuneda and K. Hirao, *J. Chem. Phys.*, 2007, **126**, 154105; (d)L. Deng, V. Branchadell and T. Ziegler, *J. Am. Chem. Soc.*, 1994, **116**, 10645.
- (a)W. Yang, Y. Zhang and P. W. Ayers, *Phys. Rev. Lett.*, 2000, **84**, 5172; (b)J. P. Perdew, R. G. Parr, M. Levy and J. L. Balduz, Jr., *Phys. Rev. Lett.*, 1982, **49**, 1691.
- D. Wang, D. Choi, Z. Yang, V. V. Viswanathan, Z. Nie, C. Wang, Y. Song, J.-G. Zhang and J. Liu, *Chem. Mater.*, 2008, **20**, 3435.
- A. Vittadini, A. Selloni, F. P. Rotzinger and M. Grätzel, *Phys. Rev. Lett.*, 1998, **81**, 2954.
- X.-Q. Gong and A. Selloni, *Phys. Rev. B*, 2007, **76**, 235307.
- A. El Goresy, M. Chen, P. Gillet, L. Dubrovinsky, G. Graup and R. Ahuja, *Earth Planet. Sci. Lett.*, 2001, **192**, 485.
- T. Ohno, K. Sarukawa and M. Matsumura, *New J. Chem.*, 2002, **26**, 1167.